Inorganic Chemistry
Article

Inorg. Chem. **2009**, *48*, 5403–5411 **5403**
DOI: 10.1021/ic900383d

Centric and Non-centric $Ca_3Au_{\sim 7.5}Ge_{\sim 3.5}$: Electron-Poor Derivatives of La_3Al_{11}. Syntheses, Structures, and Bonding Analyses

Qisheng Lin and John D. Corbett*

Ames Laboratory, USDOE, and Department of Chemistry, Iowa State University, Ames, Iowa 50011

Received February 24, 2009

Two La_3Al_{11} type derivatives have been discovered in the Ca−Au−Ge system and structurally characterized by single-crystal X-ray diffraction. Compositions $Ca_3Au_{7.16(6)}Ge_{3.84(6)}$ (**1**) and $Ca_3Au_{7.43(9)}Ge_{3.57(9)}$ (**2**) lie within a non-centric *Imm*2 phase region with $a \approx 4.40$ Å, $b \approx 13.06$ Å, $c \approx 9.60$ Å. The Au-richer and electron-poorer $Ca_3Au_{7.50(1)}Ge_{3.50(1)}$ (**3**) and $Ca_3Au_{8.01(1)}Ge_{2.99(1)}$ (**4**) occur within a centric *Pnnm* phase region with $a \approx 9.50$ Å, $b \approx 13.20$ Å, $c \approx 4.43$ Å. Both phases contain complex $[Au,Ge]_{11}^{6-}$ polyanionic networks made up of hexagonal and pentagonal prisms that are filled with the electropositive Ca atoms. Both 3:11 phases represent opposed $1 \times 3 \times 1$ superstructure distortions of $CaAu_2Ge_2$ ($ThCr_2Si_2$ type, *I*4/*mmm*), the structure of which has also been re-determined in this work. Linear muffin-tin-orbital (LMTO) calculations reveal that the symmetry variations induced by changes of the Au contents in the present 3:11 phases are consequences of bonding and structural optimizations. The hypothetical "$CaAu_{2.33-2.67}Ge_{1.33-1.00}\square_{0.33}$" compositions, which are close to those of **1**−**4**, follow through creation and elimination of vacancies within the electronegative networks of $CaAu_2Ge_2$.

Introduction

In recent years, polar intermetallics have attracted extensive attention.[1−8] Polar intermetallics are loosely referred to as electron-poor relatives of Zintl phases in which the active metals, especially those in groups 2 or 3, do not always simply contribute their valence electrons to a Zintl anion; instead, they usually participate in more delocalized bonding with the more electronegative components, typically late-transition and *p*-block metals.[9] Thus bonding motifs in polar intermetallics represent intermediate patterns between those of semiconducting Zintl phases and metal alloys, and the classic octet and Wade−Mingos rules[10] suitable for Zintl phases no longer apply for electron counting purposes.

After years of exploration for novel quasicrystal (QC) and approximant crystal (AC) phases,[11−14] we have discovered that new polar intermetallics with unprecedented structural motifs can also be uncovered in the neighborhood of such quasicrystal compounds. For example, $Mg_{35}Cu_{24}Ga_{53}$[15] was discovered during an electronic tuning of $Mg_2Cu_6Ga_5$ aimed at the QC. This is a face-centered-cubic phase featuring interpenetrating Bergman-type clusters or, in another viewpoint, a clathrate II type framework containing the electropositive Mg. Similarly, $Sc_4Mg_{0.50(2)}Cu_{14.50}Ga_{7.61(2)}$,[16] a novel incommensurate phase related to the Sc−Mg−Cu−Ga icosahedral QC, was obtained during $Sc_{x/3}Mg_{2-x/3}Cu_6Ga_5$ searches, and $Ca_4Au_{10}In_3$[17] was discovered during $CaAu_xIn_{6-x}$ reactions designed to produce a Ca−Au−In QC. The structure of the latter exhibits novel wavy Au layers separated by In and Ca. Also $CaAu_3Ga$[18] was discovered during in the electronic tuning process that led to the Ca−Au−Ga icosahedral QC. These discoveries have not only helped us to understand structural and compositional kinships between polar intermetallics and QCs/ACs, but they have also both opened new ways to access them and provided the new relationships among Hume−Rothery,[19] polar intermetallic, and Zintl phases.

*To whom correspondence should be addressed. E-mail: jcorbett@iastate.edu.

(1) Amerioun, S.; Haussermann, U. *Inorg. Chem.* **2003**, *42*, 7782.
(2) Corbett, J. D. *Angew. Chem., Int. Ed.* **2000**, *39*, 670.
(3) Corbett, J. D. In *Chemistry, Structure, and Bonding of Zintl Phases and Ions*; Kauzlarich, S. M., Ed.; VCH: New York, **1996**; p 139.
(4) Dai, J.-C.; Corbett, J. D. *Inorg. Chem.* **2007**, *46*, 4592.
(5) Haussermann, U.; Amerioun, S.; Eriksson, L.; Lee, C.-S.; Miller, G. J. *J. Am. Chem. Soc.* **2001**, *124*, 4371.
(6) Hlukhyy, V.; Raif, F.; Claus, P.; Fassler, T. F. *Chem.—Eur. J.* **2008**, *14*, 3737.
(7) Mao, J.-G.; Guloy, A. M. *J. Alloys Compd.* **2004**, *363*, 143.
(8) Seo, D.-K.; Corbett, J. D. *J. Am. Chem. Soc.* **2000**, *122*, 9621.
(9) Miller, G. J.; Lee, C.-S.; Choe, W. In *Inorganic Chemistry Highlights*; Meyer, G., Naumann, D., Wesemann, L., Eds.; Wiley-VCH: Weinheim, Germany, **2002**; p 21.
(10) (a) Wade, K. *Adv. Inorg. Chem. Radiochem.* **1976**, *18*, 1. (b) Mingos, D. M. P. *J. Chem. Soc., Chem. Commun.* **1983**, 706.
(11) Lin, Q.; Corbett, J. D. *Inorg. Chem.* **2003**, *42*, 8762.
(12) Lin, Q.; Corbett, J. D. *Inorg. Chem.* **2008**, *47*, 7651.
(13) Lin, Q.; Corbett, J. D. *J. Am. Chem. Soc.* **2007**, *129*, 6789.
(14) Lin, Q.; Corbett, J. D. *J. Am. Chem. Soc.* **2005**, *127*, 12786.
(15) Lin, Q.; Corbett, J. D. *Inorg. Chem.* **2005**, *44*, 512.
(16) Lin, Q.; Lidin, S.; Corbett, J. D. *Inorg. Chem.* **2008**, *47*, 1020.
(17) Lin, Q.; Corbett, J. D. *Inorg. Chem.* **2007**, *46*, 8722.
(18) Lin, Q.; Corbett, J. D. *Inorg. Chem.* **2008**, *47*, 3462.
(19) Hume-Rothery, W. *J. Inst. Met.* **1926**, *35*, 295.

Published on Web 05/13/2009

Table 1. Loaded Reactions, Reaction Conditions, Dominant Phases in Products, and Lattice Parameters.

loaded Ca/Au/Ge	reaction cond.[a]	products in powder pattern[b]	latt. para. for $Ca_3(Au,Ge)_{11}$ types *a, b, c* (Å), *Vol* (Å^3)[c]	cryst. code
3/7.5/4.5	A	40% $Ca_3(Au,Ge)_{11}$ + 20% $Ca_3(Au,Ge)_{19}$ + 40% $Ca(Au,Ge)_2$	4.3987 (4), 13.060 (1), 9.6032 (9), 551.67(6)	**1**
3/8.25/3.75	A	50% $Ca_3(Au,Ge)_{11}$ + 10% $Ca_3(Au,Ge)_{19}$ + 30% $CaAu_3Ge$ + 10% $Ca(Au,Ge)_2$	9.5186 (8), 13.176 (1), 4.4270 (4), 555.21 (6)	
3/6/5	A	10% $Ca_3(Au,Ge)_{11}$ + 35% $CaAu_2Ge_2$ + 20% $Ca_3(Au,Ge)_{19}$ + 35% $Ca(Au,Ge)_2$	4.4036 (4), 13.064 (1), 9.5777 (8), 550.97 (6)	
3/7/4	A	50% $Ca_3(Au,Ge)_{11}$ + 15% $Ca_3(Au,Ge)_{19}$ + 35% $Ca(Au,Ge)_2$	4.4032 (4), 13.065 (1), 9.5768 (8), 550.95 (6)	**2**
3/8/3	A	20% $Ca_3(Au,Ge)_{11}$ + 30% $CaAu_3Ge$ + 50% $Ca(Au,Ge)_2$	9.4577 (8), 13.2573 (7), 4.4410 (4), 556.82 (4)	**4**
3/7/4	B	95% $Ca_3(Au,Ge)_{11}$ + 5% $Ca_3(Au,Ge)_{19}$	4.4093 (1), 13.0731 (4), 9.5692 (3), 551.59 (2)	
3/7.5/3.5	B	80% $Ca_3(Au,Ge)_{11}$ + 20% $Ca_3(Au,Ge)_{19}$	9.5437(4), 13.1311(4), 4.4214(2), 554.09(2)	**3**
3/8/3	B	70% $Ca_3(Au,Ge)_{11}$ + unknown	9.4443(3), 13.2371(3), 4.4425(1), 555.38(1)	
3/8.5/2.5	B	60% $Ca_3(Au,Ge)_{11}$ + 40% $CaAu_3Ge$	9.3342(4), 13.3312(4), 4.4653(1), 555.65(2)	

[a] A: heated at 850 °C for 1 day, cooled to 400−500 °C at a rate of 2 °C/h, annealed there for 3 weeks; B, arc melted, then annealed at 630 °C for 1 week. [b] $Ca_3(Au,Ge)_{11}$: the title phases; $Ca_3(Au,Ge)_{19}$,[20] a new phase with YCd_6 type structure but with Wyckoff 8a site fully occupied, see also $Ca_3(Au,Ga)_{19}$;[16] $CaAu_3Ge$, a new phase isostructural with recently reported $CaAu_3Ga$;[18] $Ca(Au,Ge)_2$, a solid solution with Ca/Au/Ge around 1:1:1 in space group *Imm*2.[36] [c] From powder diffraction data; and standard settings for both structures were given.

As we followed the fecundity of Ca−Au−Ga/In QC systems[12,13] and turned to the neighboring Ca−Au−Ge/Sn systems, we again found not only QC and ACs[20] but also the title phases derived from the La_3Al_{11} structural type.[21] In recent years, many new phases related to La_3Al_{11} have become available: Sr_3In_{11},[1,7] K_3Hg_{11},[22] the $R_3(M,Tr)_{11}$ family (R = rare-earth metal, M = Ni, Cu, Zn, Ag, or Au, Tr = Al or Ga),[23−31] and the stannides $R_3M_6Sn_5$ (R = Y, Nd, Sm, Gd−Yb, M = Co, Cu).[32,33] However, no germanide has been reported, and theoretical investigations have been carried out only on s-p bonded compounds[1,5,7] or on phases that have low transition metal contents.[29] Particularly, Amerioun and Haussermann[1] have discussed in detail the size and electronic factors in the structural stability of Sr_3In_{11} and other related polar s-p bonded intermetallic compounds, and Miller and co-workers[34] have considered the structural stability of La_2NiAl_7 and La_3Al_{11} with emphasis on bonding analyses. Conclusions of both studies generally also apply to the present system. In this work, we focus on the synthesis, structure, and bonding of two new types of La_3Al_{11} derivatives discovered in the Ca−Au−Ge system. The title phases are rather special because they are dominated by electron-poor Au (∼ 50−57 at. %), and thus represent polar intermetallics with even lower effective valence electron counts (*vec*) if the Au $5d^{10}$ shell is excluded.

Experimental Section

Synthesis. The starting materials were high purity elements: Ca dendrites, Au sheet, and Ge pieces (all >99.99%, Alfa-Aesar). The elements (∼400 mg in total) were weighed in a N_2-filled glovebox (H_2O < 0.1 ppm vol.) and weld-sealed under Ar into Ta containers, which were in turn enclosed in evacuated SiO_2 jacket (< 10^{-5} torr) to avoid air oxidation of the metal containers at elevated temperature.

The non-centric $Ca_3(Au,Ge)_{11}$ phase was first encountered as a minor product in a reaction with nominal composition of "$CaAu_3Ge_3$" designed to explore the phase width of the 1/1 AC $Ca_3(Au,Ge)_{19}$.[20] This had been first heated to 850 °C, held at this temperature for 24 h, cooled to 400 °C at a rate of 2 °C/h, and annealed there for 3 weeks. A preliminary single crystal structural determination established it as a novel 1 × 3 × 1 superstructure of $CaAu_2Ge_2$[35] ($ThCr_2Si_2$ type) with elemental proportions of Ca/Au/Ge = 21.4:51.1:27.5 (at. %), corresponding to the empirical formula $Ca_3Au_{7.2}Ge_{3.8}$. Therefore, mixtures with Ca/(Au + Ge) proportions of 3:12 and 3:11 (Table 1) were reacted under the same or similar conditions. (Some were annealed at 500 °C.) However, these all produced admixtures of the title phases (< 50 vol %) with others, suggesting the former do not melt congruently. Hence, nominal $Ca_3Au_xGe_{11-x}$ (x = 7.0−8.5) samples were arc melted (weight loss ∼0.6%), and then annealed at 630 °C for a week. This annealing temperature, ∼ 30−50 °C below the melting points of the title phases, was adopted in accord with our DTA analyses (below). As a result, higher yields of the targets (∼ 60−95%) were produced at different loading ratios (Table 1).

Thermal Analyses. Because the process of slow cooling to and annealing at 400−500 °C always led to multiple products, DTA data should give helpful clues about phase transition temperatures and, of course, the melting points for each component. All measurements were carried out with the aid of a PerkinElmer Differential Thermal Analyzer (DTA-7). Samples (∼20−50 mg) were typically heated under Ar to 850 °C at a rate of 10 °C/min, then cooled to 200 °C at the same rate. XRD

(20) Lin, Q.; Corbett, J. D., unpublished results.
(21) Gomes de Mesquita, A. H.; Buschow, K. H. J. *J. Alloys Compd.* **1967**, *22*, 497.
(22) Todorov, E.; Sevov, S. C. *Inorg. Chem.* **2000**, *149*, 419.
(23) Fornasini, M. L.; Manfrinetti, P.; Mazzone, D. *Intermetallics* **2007**, *15*, 856.
(24) Krachan, T.; Stel'makhovich, B. M.; Kuz'ma, Y. B. *J. Solid State Chem.* **2003**, *349*, 134.
(25) Krachan, T.; Stel'makhovich, B.; Kuz'ma, Y. B. *J. Alloys Compd.* **2005**, *386*, 147.
(26) Speka, M.; Prots', Y. M.; Belyavina, N. M.; Markiv, V. Y.; Grin', Y. *Z. Kristallogr. - New Cryst. Struct.* **2004**, *219*, 211.
(27) Stel'makhovich, B.; Stel'makhovich, O.; Kuz'ma, Y. B. *J. Alloys Compd.* **2005**, *397*, 115.
(28) Stel'makhovich, B. M.; Gumeniuk, R. V.; Kuz'ma, Y. B. *J. Alloys Compd.* **2000**, *307*, 218.
(29) Nordell, K. J.; Miller, G. J. *Angew. Chem., Int. Ed. Engl.* **1997**, *36*, 2008.
(30) Gumeniuk, R. V.; Taras, I. B.; Kuz'ma, Y. B. *J. Alloys Compd.* **2006**, *416*, 131.
(31) Stel'makhovich, B. M.; Zhak, O. V.; Bilas, N. R.; Kuz'ma, Y. B. *J. Alloys Compd.* **2004**, *363*, 243.
(32) Fornasini, M. L.; Manfrinetti, P.; Mazzone, D.; Riani, P.; Zanicchi, G. *J. Solid State Chem.* **2004**, *177*, 1919.
(33) Pottgen, R. *J. Alloys Compd.* **1995**, *224*, 14.
(34) Gout, D.; Barker, T. J.; Gourdon, O.; Miller, G. J. *Chem. Mater.* **2005**, *17*, 3661.
(35) May, N.; Schafer, H. *Z. Naturforsch.* **1972**, *27b*, 864.

patterns pre- and post-DTA scanning were also collected for phase identification. The melting points of $Ca_3(Au,Ge)_{19}$ (*Im*3),[20] $Ca(Au,Ge)_2$ (*Imm*2),[36] and the title $Ca_3(Au,Ge)_{11}$ phases (both *Imm*2 and *Pnnm*) were determined to be about 575−605 °C, 740−780 °C, and 658−683 °C, respectively. (Melting point ranges exist because the three phases are not line compounds, as also reflected by peak shifts in their powder patterns.) The DTA patterns of the nominal $Ca_3Au_7Ge_4$ and $Ca_3Au_{7.5}Ge_{3.5}$ examples that led to crystals **2** and **3** are shown in the Supporting Information, Figure S1.

Powder Diffraction. Powder diffraction data were collected on a Huber 670 Guinier powder camera equipped with an area detector and Cu Kα_1 radiation (λ = 1.540598 Å) that had been calibrated with Si standard (NIST SRM 640b). Phase identities and purities were checked with the aid of PowderCell,[37] and lattice parameters were refined by UnitCell.[38] Two-theta values of reflection peaks used for refinements of lattice parameters were automatically searched by program Winplotr.[39] The refined lattice parameters for **1**−**4** given in Table 1 were also used for bond distance calculations.

Single Crystal X-ray Diffraction. Four single crystals from different reactions (Table 1) were mounted on a Bruker APEX CCD single crystal diffractometer equipped with graphite-monochromatized Mo Kα (λ = 0.71069 Å) radiation. Intensity data were collected at room temperature in an ω scan mode within θ = ∼1.5−28 ° and with exposures of 10−30 s/frame. A total of 1315 frames, defined by a hemisphere, were collected for each data set. Data integration, Lorentz polarization, empirical absorption, and other corrections were made by SAINT and SADABS subprograms that are included in the SMART software package.[40] Full-matrix least-squares refinements on F_o^2 were performed with the aid of the SHELXTL v 6.1 program.[41]

Systemic absences suggested two crystals, **1** and **2**, had body centered lattices, and the $|E^2 - 1|$ values, ∼ 0.75, that both had non-centric symmetry. Thus three possible space groups, *I*222, $I2_12_12_1$, and *Imm*2 agree with these conditions. However, only *Imm*2 yielded satisfactory structure models, as illustrated by the structure refinements of crystal **1** in the following. The non-centric symmetry is also evident according to a map of observed electron densities along the shortest *a* axis, Supporting Information, Figure S2a, in which the mirror plane perpendicular to the *c* axis is missing.

Within the *Imm*2 symmetry, direct methods with crystal **1** data yielded seven independent sites with interatomic distances in the range of 2.34−2.90 Å, suitable for Au/Ge−Au/Ge pairs. Therefore, these positions were temporarily assigned to Au. The R1 value converged at 14.9% after several cycles of refinement, but the isotropic displacement parameters for two positions (0.071 and 0.076 Å^2) were much too large compared with those of others (0.017−0.021 Å^2), which suggested that atoms with smaller scattering powers (Ge or Au/Ge mixtures) could occupy these two positions. Hence, Ge was substituted, after which R1 decreased slightly to 12.7%, and U_{iso} values for both as Ge (0.016 and 0.022 Å^2) were now acceptable. At this stage, the difference Fourier map yielded another two weakly scattering positions that were located in cages and had shortest distances to Au of ∼ 3.02−3.09 Å, falling in the range of the Ca−Au pair distances observed in other intermetallic phases.[12,17,18,35] Apparently, both positions could be populated by Ca atoms, and they were so assigned. After a few cycles of isotropic displacement refinements, the difference Fourier map suggested that no more independent atoms were present. Meanwhile, re-examination of U_{iso} revealed that one of the Ge positions had a considerably smaller value (0.014 Å^2) compared with the others (0.020−0.026 Å^2), a clue for Au/Ge admixture at this position. The final least-squares refinements, with anisotropic displacement parameters, converged at R1 = 5.68%, wR2 = 13.75%, and GOF = 1.077; the maximum (3.93 e/Å^3) and minimum (−3.49 e/Å^3) residual peaks were both close to Au atoms (0.95−1.73 Å). The refined composition was $Ca_3Au_{7.16(6)}Ge_{3.84(6)}$. The Flack parameter refined to zero, indicating that the absolute structure had been determined. Similar situations occurred in the structural refinement of crystal **2**. The most pronounced differences between crystals **1** and **2** are that the latter contains four more Au/Ge mixed positions on former Au sites even though it is Ge-poorer than **1**. The formula of **2** was refined to be $Ca_3Au_{7.43(5)}Ge_{3.57(5)}$, with final R1 = 3.33%, wR2 = 6.49%, and GOF = 1.074, and maximal and minimal residual peaks of about 2.83 e/Å^3 and −2.64 e/Å^3, respectively.

For crystal **3** and **4**, systematic absence analyses revealed a primitive lattice and a centric space group of *Pnnm* instead. The general structure determinations and refinements for both were similar to that described for **1**. The final least-squares refinement for crystal **3**, with anisotropic displacement parameters, yielded a composition of $Ca_3Au_{7.50(1)}Ge_{3.50(1)}$, and converged at R1 = 2.59%, wR2 = 6.47%, and GOF = 1.073, with maximal and minimal residual peaks 3.46 e/Å^3 and −2.20 e/Å^3. In comparison, this process for crystal **4**, $Ca_3Au_{8.01(1)}Ge_{2.99(1)}$, converged at R1 = 3.43%, wR2 = 8.59%, and GOF = 1.122, with maximal and minimal residual peaks ∼3.61 e/Å^3 and −3.04 e/Å^3. For direct comparison with **1** and **2**, both crystallographic data sets were transformed to the non-standard setting *Pmnn*; see Supporting Information, Table S1. In the text, however, all parameters are reported in the standard setting *Pnnm*.

Some general data collection and refinement parameters and crystallographic data are given in Table 2. The refined positional and isotropic−equivalent displacement parameters for **1** and **2** are listed in Table 3, and for **3** and**4** in Table 4. All atomic positions were standardized by STRUCTURE TIDY[42] and, for comparison, pairs of atoms with *pseudo* mirror plane symmetry in the *c* direction (in **1** and **2**) were sorted together. Other crystallographic data are available in CIF outputs in the Supporting Information, in which Tables S2 and S3 contain anisotropic displacement parameters for **1** and **2**, and **3** and **4**, respectively, and Table S4 contains the important interatomic distances for all four structures.

Electronic Structure Calculations. The calculations were performed by means of the self-consistent, tight-binding, linear-muffin-tin-orbital (LMTO) method in the local density (LDA) and atomic sphere (ASA) approximations, within the framework of the DFT method.[43−46] The ASA radii for Ca, Au, and Ge were automatically scaled with a maximal overlap restriction of 16%, and interstitial spheres were introduced automatically. All atomic and empty spheres had reasonable radii. Reciprocal space integrations were carried out using the tetrahedron method. The basis sets for Ca included 3d, 4s, and 4p, for Au, 6s, 6p, and 5d, and for Ge, 4s and 4p orbitals. Down-folding techniques were applied for Ca 4p, Au 5f, and Ge 4d orbitals. Scalar

(36) Merlo, F.; Pani, M.; Canepa, F.; Fornasini, M. L. *J. Alloys Compd.* **1998**, *264*, 82.
(37) Kraus, W.; Nolze, G. *J. Appl. Crystallogr.* **1996**, *29*, 301.
(38) Holland, T. J. B.; Redfer, S. A. T. *Mineral. Mag.* **1997**, *61*, 65.
(39) Roisnel, T.; Rodríguez-Carvajal, J. *WinPLOTR: a Windows tool for powder diffraction patterns analysis*; Proceedings of the Seventh European Diffraction Conference (EPDIC 7), Delhez, R., Mittenmeijayer, E. J., Eds.; 2000, pp 118−123.
(40) *SMART*; Bruker AXS, Inc.: Madison, WI, **1996**.
(41) *SHELXTL*; Bruker AXS, Inc: Madison, WI, **2000**.
(42) Gelato, L. M.; Parthé, E. *J. Appl. Crystallogr.* **1987**, *20*, 139.
(43) Tank, R.; Jepsen, O.; Burkhardt, A.; Andersen, O. K. *TB-LMTO-ASA Program*, Vers. 4.7; Max-Planck-Institut fur Festkorperforschung: Stuttgart, Germany, **1994**.
(44) Shriver, H. L. *The LMTO Method*; Springer-Verlag: Berlin, Germany, **1984**.
(45) Jepsen, O.; Snob, M. *Linearized Band Structure Methods in Electronic Band-Structure and its Applications, Springer Lecture Note*; Springer Verlag: Berlin, Germany, **1987**.
(46) Anderson, O. K.; Jepsen, O. *Phys. Rev. Lett.* **1984**, *53*, 2571.

Table 2. Crystal and Structural Refinement Data for Crystals **1**, $Ca_3Au_{7.16(6)}Ge_{3.84(6)}$, **2**, $Ca_3Au_{7.43(9)}Ge_{3.57(9)}$, **3**, $Ca_3Au_{7.50(1)}Ge_{3.50(1)}$, and **4**, $Ca_3Au_{8.01(1)}Ge_{2.99(1)}$

	1	2	3	4
vec	28.52	27.71	27.5	25.97
formula	$Ca_3Au_{7.16(6)}Ge_{3.84(6)}$	$Ca_3Au_{7.43(5)}Ge_{3.57(5)}$	$Ca_3Au_{7.50(1)}Ge_{3.50(1)}$	$Ca_3Au_{8.01(1)}Ge_{2.99(1)}$
formula weight	1809.3	1842.9	1851.6	1915.0
cryst. system		orthorhombic		
space group, Z	*Imm*2, 2	*Imm*2, 2	*Pnnm*, 2	*Pnnm*, 2
unit cell (Å)				
a	4.3987(8)	4.4154 (6)	9.5598(9)	9.4577(8)
b	13.060(1)	13.100 (2)	13.1311(4)	13.2573(7)
c	9.6032(9)	9.577 (1)	4.4214(2)	4.4410(4)
vol. (Å^3)	551.7(1)	554.0 (1)	555.02(6)	556.83(7)
d_{cal} (g/cm^3)	10.89	11.05	11.08	11.42
abs.coeff.(mm^{-1})	106.421	108.82	109.35	114.33
refl. coll. /R(int)	1139/0.0559	1738/0.0440	3314/0.0409	3318/0.0513
data/restr./para.	537/1/49	641/1/54	738/0/47	740/0/47
GOF on F^2	1.096	1.074	1.073	1.122
R1/wR2 [$I > 2\sigma(I)$]	0.0568/0.1360	0.0330/0.0649	0.0259/ 0.0647	0.0343/ 0.0859
[all data]	0.0582/ 0.1370	0.0357/0.0661	0.0312/ 0.0674	0.0462/ 0.0908
residues (e Å^{-3})	3.93/−3.49	2.83/−2.64	3.46/−2.20	3.61/−3.04

Table 3. Atomic Coordinates and Equivalent Isotropic Displacement Parameters for Crystals **1**, $Ca_3Au_{7.16(6)}Ge_{3.84(6)}$, and **2**, $Ca_3Au_{7.43(5)}Ge_{3.57(5)}$, Listed in Sequence

atom[a]	Wyck.	symm.	occ. (≠1)[b]	x	y	z	U_{iso} (Å^2)
M1	2*a*	*mm*2		0	0	0.5048(3)	0.023(1)
			0.93/0.07(1)	0	0	0.5000(2)	0.015(1)
Au2	2*b*	*mm*2		0	1/2	0.2030(3)	0.022(1)
				0	1/2	0.1980(2)	0.015(1)
Au3	2*b*	*mm*2		0	1/2	0.8156(3)	0.025(1)
				0	1/2	0.8069(2)	0.018(1)
M4	4*d*	*m*..		0	0.3415(2)	0.6229(2)	0.023(1)
			0.87/0.13(1)	0	0.3413(1)	0.6169(2)	0.019(1)
M5	4*d*	*m*..		0	0.3210(4)	0.3617(5)	0.018(1)
			0.16/0.84(1)	0	0.3249(2)	0.3632(3)	0.030(1)
M6	4*d*	*m*..		0	0.8667(2)	0.7441(2)	0.019(1)
			0.90/0.10(1)	0	0.8661(1)	0.7372(1)	0.013(1)
M7	4*d*	*m*..	0.08/0.92(2)	0	0.8681(4)	0.2797(4)	0.019(2)
			0.32/0.68(1)	0	0.8664(2)	0.2720(2)	0.020(1)
Ca1	2*a*	*mm*2		0	0	0	0.025(3)
				0	0	0	0.017(2)
Ca2	4*d*	*m*..		0	0.3090(8)	0.007(1)	0.022(2)
				0	0.3099(4)	0.0024(8)	0.014(1)

[a] M = Au/Ge. [b] Separate refinements with Au/Ge admixtures at M1−M7 in **1** indicated that M7 is the only mixed site, whereas M1−M5 are pure Au, and M6, pure Ge.

Table 4. Atomic Coordinates and Equivalent Isotropic Displacement Parameters for Crystals **3**, $Ca_3Au_{7.50(1)}Ge_{3.50\ (1)}$, and **4**, $Ca_3Au_{8.01(1)}Ge_{2.99(1)}$

Atom[a]	Wyck.	Symm.	Occ. (≠1)	x	y	z	U_{iso} (Å^2)
Au1	2*a*	..2/*m*		0	0	0	0.015(1)
				0	0	0	0.018(1)
Au2	4*g*	..*m*		0.3016(1)	0.4969 (1)	0	0.013(1)
				0.2988(1)	0.4967(1)	0	0.014(1)
Au3	4*g*	..*m*		0.1122(1)	0.6584(1)	0	0.015(1)
				0.1108(1)	0.6595(1)	0	0.016(1)
Ge4	4*g*	..*m*		0.1478(2)	0.3168(1)	0	0.011(1)
				0.1517(2)	0.3170 (2)	0	0.012(1)
Au5	4*g*	..*m*		0.7605(1)	0.1380(1)	0	0.012(1)
				0.7623(1)	0.1364(1)	0	0.013(1)
M6	4*g*	..*m*	0.251/ 0.749(5)	0.2229(1)	0.1274(1)	0	0.013(1)
			0.506/ 0.496(7)	0.2218(1)	0.1299(1)	0	0.015(1)
Ca1	2*d*	..2/*m*		0	1/2	1/2	0.015(1)
				0	1/2	1/2	0.016(2)
Ca2	4*g*	..*m*		0.4995(3)	0.3108(3)	0	0.012(1)
				0.5018(4)	0.3105(4)	0	0.012(1)

[a] M = Au/Ge.

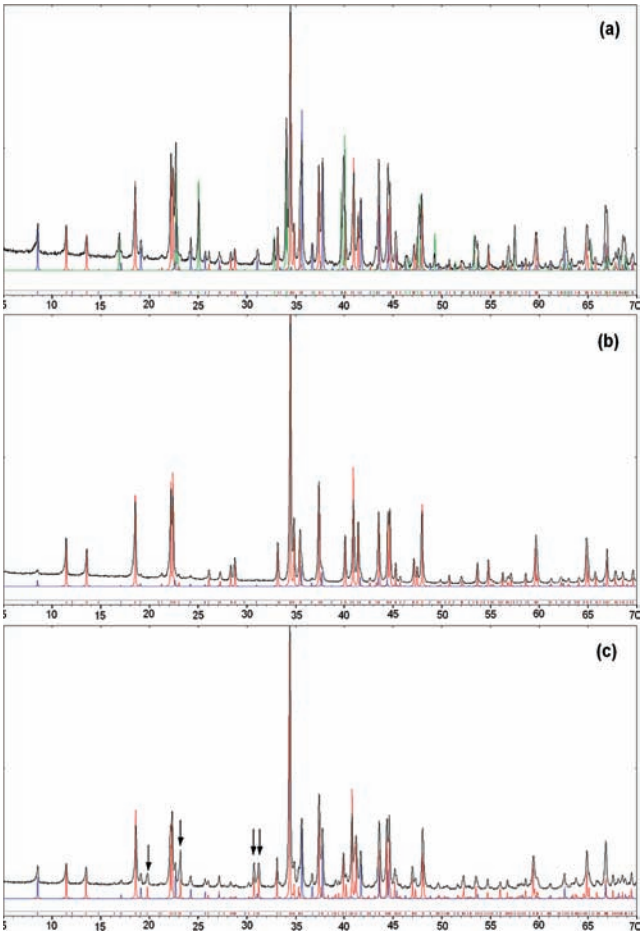

Figure 1. Observed (black) powder patterns for products of nominal $Ca_3Au_7Ge_4$ after (a) slow cooling and 500 °C annealing, (b) arc melting and 630 °C annealing, and (c) $Ca_3Au_{7.5}Ge_{3.5}$ after arc melting and annealing at 630 °C, together with patterns calculated (red) from single crystal data for crystal **1** (*Imm*2) in (a) and (b), and of **3** (*Pnnm*) in (c). Powder patterns for the minor products $Ca_3(Au,Ge)_{19}$, blue, and $Ca(Au,Ge)_2$ (*Imm*2), green, are also drawn. Arrows in (c) mark the major differences in powder diffraction between the non-centric *Imm*2 and centric *Pnnm* phases.

relativistic effects were included in the calculations. The crystal overlap Hamilton population (COHP)[47] analyses were performed to gain insight into the bonding properties.

(47) Dronskowski, R.; Bloch, P. *J. Phys. Chem.* **1993**, *97*, 8617.

Results and Discussion

Phase Separation and Synthesis. Figure 1 a−c shows the experimental powder patterns (black) of nominal $Ca_3Au_7Ge_4$ after (a) slow cooling and annealing (500 °C), (b) arc melting and annealing (630 °C), and (c) of $Ca_3Au_{7.5}Ge_{3.5}$ after arc melting and annealing at 630 °C. Patterns calculated from the respective single crystal data are also included. First, let us look at the difference between these fFigures. Figure 1c exhibits several additional reflections that are not in 1a and 1b, for example, those at $2\theta \sim 19.7°$, 23.2 , 30.7°, 31.2° (marked by arrows). Such differences illustrate that the $Ca_3(Au,Ge)_{11}$ products in nominal $Ca_3Au_7Ge_4$ (a, b) and $Ca_3Au_{7.5}Ge_{3.5}$ (c) reactions have different symmetries and are consistent with the simulated patterns (red). According to our synthetic results (Table 1), crystals **2** and **3** appear to be close to their phase boundaries, in equilibrium with the adjoining phases. In other words, the composition of crystal **2** is very close to the upper limit of the non-centric $Ca_3(Au,Ge)_{11}$ (*Imm*2) solid solution, and **3**, to the lower limit of the centric $Ca_3(Au,Ge)_{11}$ (*Pnnm*), as supported by the refined compositions for **2** and **3** in the single crystal analyses (Table 2).

According to Figure 1a, the nominal $Ca_3Au_7Ge_4$ composition contained three phases after cooling and annealing at 500 °C, $Ca_3(Au,Ge)_{11}$ (*Imm*2), $Ca_3(Au,Ge)_{19}$ (*Im*3),[20] and $Ca(Au,Ge)_2$ (*Imm2*).[36] However, the last phase disappeared upon annealing at 630 °C, and the yield of the cubic $Ca_3(Au,Ge)_{19}$ (*Im*3) also decreased from 15% to ∼5%. These suggest a peritectic formation on cooling: $Ca_3(Au,Ge)_{19}$ (*Im*3) + $Ca(Au,Ge)_2$ (*Imm*2) → $Ca_3(Au,Ge)_{11}$ (*Imm*2). In addition, the reverse reaction, a decomposition of $Ca_3(Au,Ge)_{11}$ into $Ca(Au,Ge)_2$ and $Ca_3(Au,Ge)_{19}$, is seen according to powder patterns before and after DTA measurements (Supporting Information, Figure S1).

However, according to our experiments, no phase transition occurs between the non-centric *Imm*2 and the centric *Pnnm* symmetry (or the reverse) on temperature variation at a fixed composition ; rather, this change occurs only when the composition is varied. For example, the $Ca_3(Au,Ge)_{11}$ products in $Ca_3Au_7Ge_4$ reactions were always found crystallizing in the non-centric *Imm*2 symmetry, regardless of the thermal history of samples, as seen in Figures 1a, 1b and S1. Similarly, the $Ca_3(Au,Ge)_{11}$ products in nominal $Ca_3Au_{7.5}Ge_{3.5}$ reactions were always found in the centric *Pnnm* symmetry (Figure 1c and Supporting Information, Figure S1).

Crystal Structures. Both the non-centric *Imm*2 and centric *Pnnm* title phases are novel variants of the well-known parent structure of La_3Al_{11} (*Immm*).[21] The last type appears for several dozen representatives,[48] most of them ternary compounds consisting of an active metal (groups 1−3), a late transition metal, and Al or Ga, whereas binary examples generally contain an active metal and Al or its neighbors, Zn and In. A few ternary indides and stannides are also available, but they occur as distorted, symmetry-lowered, or defect-ordered variants, for example, $La_3Au_4In_7$ ($I2/m$)[49] and $Ln_3Co_6Sn_5$ (Ln = Y, Nd, Sm, Gd−Tm) (*Immm*).[33]

In contrast to crystals **3** and **4** and their parent La_3Al_{11}, the absence of centro-symmetry for **1** and **2** is clear. The average R_{int} and R_{sigma} factors for both crystals are about 0.05, indicating high quality data sets. The refined coordinates z_{Au1}, $(z_{Au2} + z_{Au3})/2$, $(z_{M4} + z_{M5})/2$, and $(z_{M6} + z_{M7})/2$, all deviate from 1/2 by at least 16 σ, whereas z_{Ca2} is different from zero by 7 σ (Ca1 was restrained to the origin), Table 3, indicating that the deviations from mirror symmetry along *c* are definite. Therefore, it was not surprising that pairs of split positions (or elongated displacement parameters) appeared during attempted structural solutions for **1** and **2** in the *Immm* space group. Also, the interatomic distances for d_{M1-Au2} versus d_{M1-Au3}, d_{M4-M6} versus d_{M5-M7}, d_{Au3-M4} versus d_{Au2-M5}, and d_{M1-M6} versus d_{M1-M7} (M = Au, Ge, or Au/Ge) differ appreciably, Supporting Information, Table S4.

Panels a−c in Figure 2 show the structures of $CaAu_2Ge_2$ ($I4/mmm$)(3 cells), $Ca_3Au_{7.16}Ge_{3.84}$ (*Imm*2), and $Ca_3Au_{8.0}Ge_{3.0}$ (*Pnnm*), respectively. In $CaAu_2Ge_2$,[35] the basal Au atoms (Wyckoff 4*d* site) form square nets that are alternatively capped above and below the plane by the apical Ge atoms (4*e* site), resulting in layers of alternating square pyramids. Because of strong Ge−Ge interlayer bonding along *c* (as suggested by the COHP data, below), neighboring layers of square pyramids are linked together to form a three-dimensional electronegative $[Au_2Ge_2]^{2-}$ network wherein the Ca countercations fill the resulting hexagonal prisms. In the 3:11 phases, no Ge−Ge interlayer bond exists any more; rather, the former Ge−Ge pairs in $CaAu_2Ge_2$ have now been replaced by single atoms (Au1) on distortion, Figures 2b and 2c. As a result, the rearranged polyanionic networks bear the features of both $CaAu_2Ge_2$[35] and Ba_2AuTl_7.[50] That is, they exhibit alternating distorted hexagonal (motif of $CaAu_2Ge_2$) and pentagonal prisms (of Ba_2AuTl_7), in which cages are filled by Ca1 and Ca2, respectively. (In comparison, the $[AuTl_7]^{4-}$ polyanions in Ba_2AuTl_7 condense into a complex network containing two types of pentagonal prisms.) Within the polyanionic networks, interatomic Au/Ge distances (Supporting Information, Table S4) fall in the range of 2.52−2.96 Å in **1** and 2.44−2.94 Å in **2**, 2.50 −2.94 Å in **3**, and 2.50 −2.96 Å in **4**, typical for Au/Ge−Au/Ge bonds, such as from the sums of Pauling's single bond metallic radii, 2.58 Å (Au: 1.339 Å, Ge: 1.242 Å).[51]

Now let us discuss the environments of the active metal Ca in **1** and **2** and **3** and **4**. The Ca1 atoms in both structural types lie in distorted polyhedra that are comparable to those in $CaAu_2Ge_2$, that is, 16-vertex polyhedra with characteristic hexagonal prisms along *a* plus four waist atoms (Figure 2 b and 2c). Ca1 atoms in **1** and **2** have $2/m$ symmetry, and in **3** and **4**, *mm*2 symmetry. The distortion of the polyhedra about Ca1 between the two types of structures is noteworthy, for example, in **1** and **2**, d_{Ca1-M4} and d_{Ca1-M5} differ less than 0.23 Å, whereas the

(48) Villars, P.; Calvert, L. D. *Pearson's Handbook of Crystallographic Data for Intermetallic Phases*, 2nd ed.; American Society of Metals: Materials Park, OH, **1991**; Vol. *1*.

(49) Galadzhun, Y. V.; Zaremba, V. I.; Kalychak, Y. M.; Hoffmann, R. D.; Pottgen, R. *Z. Anorg. Allg. Chem.* **2000**, *626*, 1773.

(50) Liu, S.; Corbett, J. D. *Inorg. Chem.* **2004**, *43*, 2471.

(51) Pauling, L. *The Nature of the Chemical Bond.* 3rd ed.; Cornell University Press: Ithaca, **1960**; p 403.

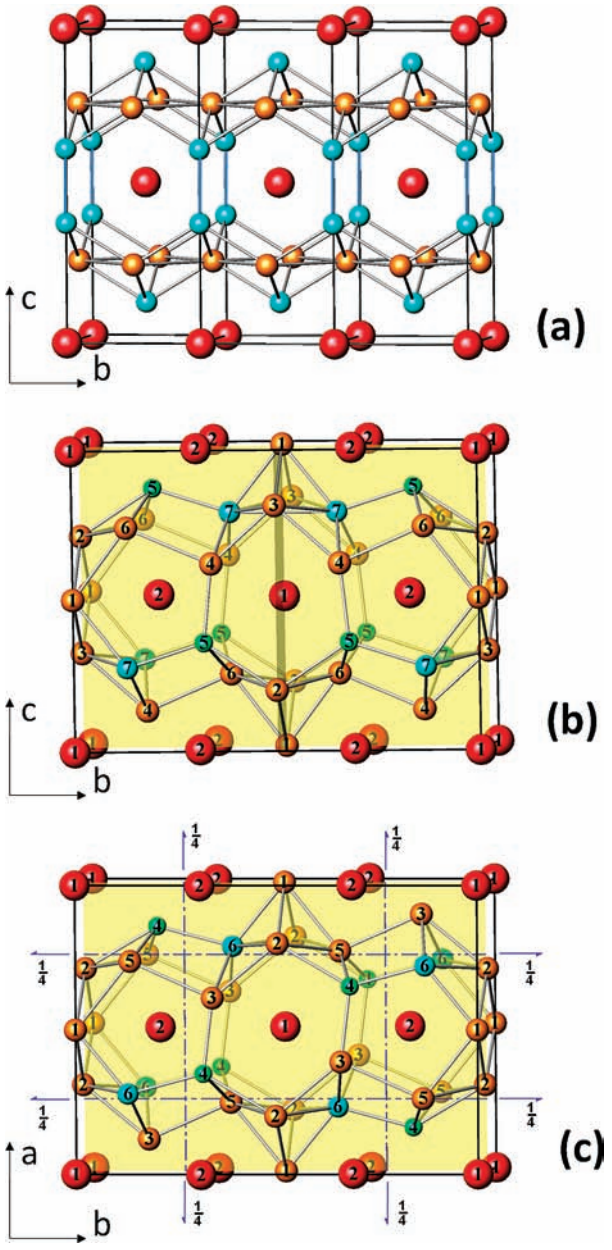

Figure 2. Crystal structures of (a) tripled $CaAu_2Ge_2$ cells (*I*4/*mmm*), (b) $Ca_3Au_{7.16}Ge_{3.84}$ (*Imm*2), and (c) $Ca_3Au_{7.50}Ge_{3.50}$ (*Pnnm*). For direct comparisons, the origin in (c) has been shifted by (0, 1/2, 1/2) to the Ca1 position. Ca atoms are represented by red, Au by golden, Ge by cyan, and Au/Ge by green spheres. Mirror planes in (b) and (c) are yellow, and the *n* glide positions in (c) are also shown.

difference for corresponding pairs ($d_{Ca1-Au3}$ and $d_{Ca1-Ge4}$) in **3** and **4** are larger than 0.34 Å. In contrast, Ca2 atoms in both structure types have mirror symmetry (Tables 3 and 4), and all have coordination spheres comparable to that for Ba in Ba_2AuTl_7,[50] featuring pentagonal prisms along the shortest axial direction. Similar coordination polyhedra are also found about Sr in monoclinic $SrIn_4$.[8]

Group-Subgroup Relationships. The group−subgroup relationships between $CaAu_2Ge_2$ (*I*4/*mmm*, $ThCr_2Si_2$-type) and crystals **1** and **2** (*Imm*2) and **3** and **4** (*Pnnm*) are shown in Figure 3 together with their relationships to La_3Al_{11} (*Immm*). From the viewpoint of group theory, there is no direct *translationengleiche* or *klassengleiche*[52,53] relation from the aristotypic $CaAu_2Ge_2$ (*I*4/*mmm*) to either the centric $Ca_3(Au,Ge)_{11}$(*Pnnm*) or the non-centric $Ca_3(Au,Ge)_{11}$ (*Imm*2). Rather, the pathway must go through at least two intermediate stages, for example, via a *translationengleiche* symmetry reduction of index 2 (t2) from *I*4/*mmm* to *Immm* followed by an isomorphous subgroup transformation to realize the tripled unit cell (i3). Therefore, dashed lines are used from $CaAu_2Ge_2$ (*I*4/*mmm*) to $Ca_3(Au,Ge)_{11}$ (*Immm*) [represented by its parent La_3Al_{11} (*Immm*) in Figure 3]. Note, however, that this does *not* mean the intermediate $Ca_3(Au,Ge)_{11}$ (*Immm*) phase must exist. The transition from the intermediate $Ca_3(Au,Ge)_{11}$ (*Immm*) phase to the centric $Ca_3(Au,Ge)_{11}$ (*Pnnm*) takes a symmetry reduction of *klassengleiche* (k2), which is new in the La_3Al_{11} family, whereas the path to $Ca_3(Au,Ge)_{11}$ (*Imm2*) requires a *translationengleiche* (t2). However, there is no group−subgroup relationship between the centric *Pnnm* and the non-centric *Imm*2 symmetries. This agrees with experimental observations that no temperature-dependent symmetry change is found for $Ca_3(Au,Ge)_{11}$ once its starting composition is fixed (above). Actually, such a discontinuous change is also reflected in the distribution of Au/Ge mixed sites (Tables 3 and 4): the number of independent mixed sites increases from one to five from crystal **1** to **2**; however, this trend does not continue from **2** to **3**. In addition, the different pathways taken during puckering of the Au layers, compare Figures 2b and 2c, also suggest that a direct phase transition between the two phases is not possible. Taking the puckering of Au layers at $c \approx 3/4$ in Figure 2b and $a \approx 3/4$ in Figure 2c as examples, although both layers are waved along the *b* axes, the *z* atomic positions relative to $z = 3/4$ for the former layer (2 → 6 → 4 → 3 → 4 → 6 → 2) vary as "− − − + − − −"; in contrast, *x* varies as "− − − + + + −" for the latter (2 → 5 → 3 → 2 → 5 → 3 → 2). ("+" means $x, z > 3/4$, and "−", $x, z < 3/4$.)

Electronic and Size Factors. Similar to other polar intermetallics, the structure stability of these $Ca_3(Au,Ge)_{11}$ phases involves a complicated interplay between electronic, size, and packing factors.[1,5] A survey of the La_3Al_{11}-related compounds reveals that this structural derivative allows a much larger valence electron count (*vec*) range than does its parent $ThCr_2Si_2$. The latter type is observed with 36−42 *vec* per *three* formula units (for direct comparison with the La_3Al_{11} type).[5] In contrast, the *vec* values for La_3Al_{11} types presently span from K_3Hg_{11} (25)[22] through $Yb_3Au_{4.7}Ga_{6.3}$ (29.6),[54] $La_3Au_4Al_7$ (34),[49] $Dy_3Au_2Al_9$ (38),[29] to La_3Al_{11} (42).[21] The reason is because many structures with smaller values contain electron-poorer late transition metals such as Cu, Ag, Au, Hg, Co, Ni, and Pt with an implied participation of filled d^{10} orbitals in bonding. The *vec* values per formula unit for the title phases fall between 28.5 for **1** and 26.0 for **4** (without counting the Au $5d^{10}$ electrons). Nevertheless, crystal **4** has the lowest *vec* value for a ternary compound in the La_3Al_{11} family.

(52) Muller, U. *Inorganic Structural Chemistry*; John Wiley & Sons: Chichester, **1993**.

(53) Barnighausen, H. *Commun. Math. Chem.* **1980**, *9*, 139.

(54) Grin', Y.; Ellner, M.; Hiebl, K.; Rogl, P.; Sichevich, O. M.; Myakush, O. M. *J. Alloys Compd.* **1994**, *205*, 285.

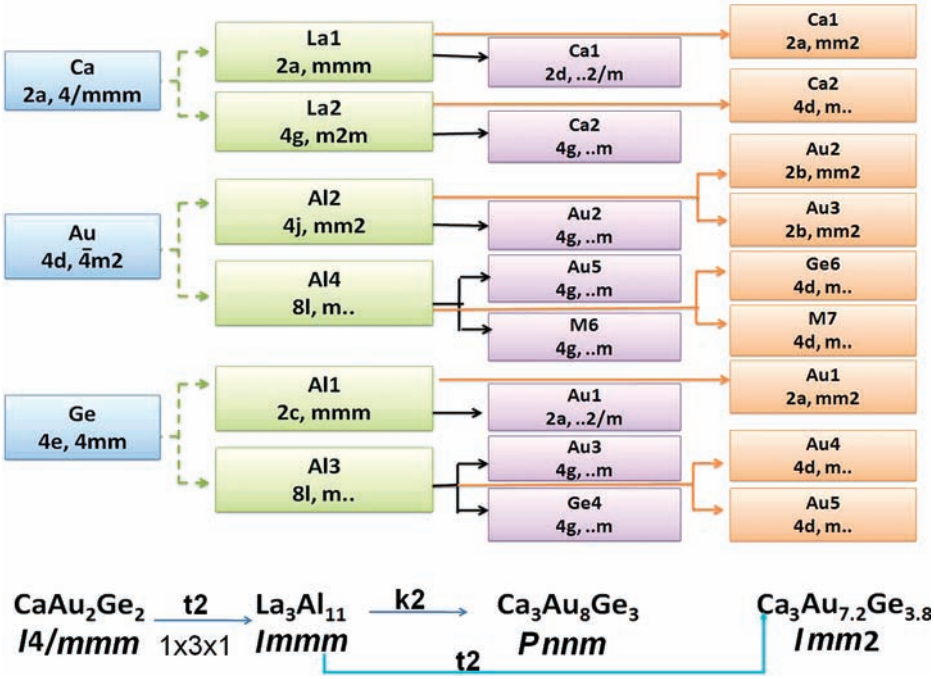

Figure 3. Group-subgroup relationships among $CaAu_2Ge_2$ (*I*4/*mmm*), La_3Al_{11} (*Immm*), and the title non-centric (*Imm*2) and centric (*Pnnm*) $Ca_3(Au, Ge)_{11}$ phases. t2 means a *translationengleiche* symmetry reduction of index 2, and k2, a *klassengleiche* reduction of index 2.[52,53]

Size and packing effects also play important roles in structural selection among the La_3Al_{11} type phases, and these sometimes appear to override the electronic factors. For example, replacement of Ge by electron-poorer Ga gives $Ca_3Au_{6.6}Ga_{4.4}$ (*vec* = 25.8)[55] with the same 3:11 stoichiometry. However, this does not show the La_3Al_{11} structural motif; rather, chains of face-shared $[Au_6Ga_6]$ icosahedra are linked by mixed Au/Ga spacers. If Yb replaces Ca, then $Yb_3Au_{4.7}Ga_{6.3}$ [54] (*vec* = 29.6) forms in the La_3Al_{11} type again, but if Ge is replaced by the larger Sn, the 3:11 type structure does not appear to exist in the Ca−Au−Sn system.[20]

Electronic Structure and Bonding. The electronic structures of s-p bonded $ThCr_2Si_2$-type compounds are relatively well understood.[5,34] However, it remains instructive to first take a look at the electronic structure of $CaAu_2Ge_2$ because it contains a large fraction of Au for which the influence of 5d electrons cannot be neglected. Moreover, the Au and Ge distribution in $CaAu_2Ge_2$[35] appears to contradict the general postulates from Mulliken population analyses[56] or "coloring" analyses[5] of s-p bonded $ThCr_2Si_2$-type compounds. That is, those atoms with smaller electronegativities and larger sizes generally tend to occupy the so-called basal or planar sites (Wyckoff 4*d*), whereas the apical sites (4*e*) are favored for the stronger bonds and atoms of larger electronegativity (Mulliken electronegativities for Au and Ge are 5.77 and 4.6 eV[57]). Therefore, the electronic structures of different versions of $CaAu_2Ge_2$ were calculated on the basis of our own crystallographic data,[58] and the results indicated that Au at the basal position yields ~0.70 eV lower total energy compared with the inverse structure

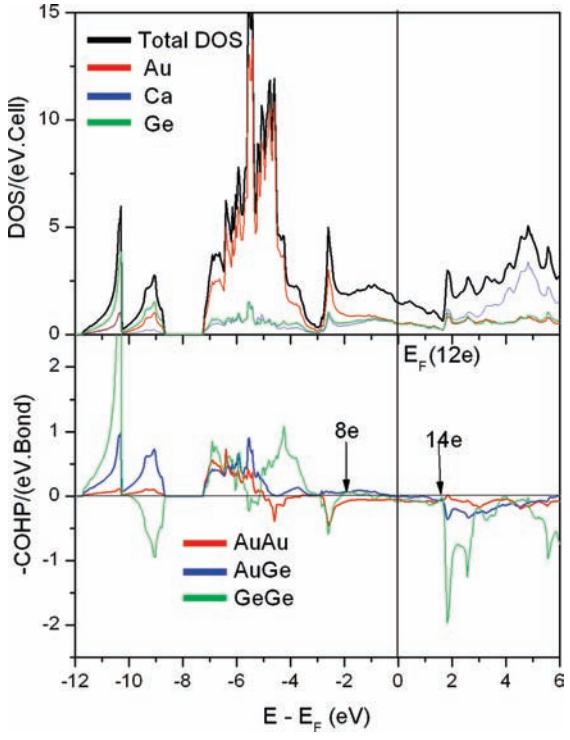

Figure 4. Densities-of-states (DOS) and crystal overlap Hamilton population (COHP) data for $CaAu_2Ge_2$.

(55) Cordier, R.; Roehr, C.; Kussmann, D.; Hoffmann, R. D.; Pottgen, R. *Z. Anorg. Allg. Chem.* **2001**, *627*, 2053.
(56) Miller, G. J. *Eur. J. Inorg. Chem.* **1998**, *5*, 523.
(57) Pearson, R. G. *Inorg. Chem.* **1988**, *27*, 734.
(58) Reactions with nominal $CaAu_xGe_{4-x}$ compositions (x = 1.33, 2.0, 2.67, and 3.33) were run to check for the presence of "coloring problems" (see text) with $CaAu_2Ge_2$. Powder diffraction analyses revealed that $CaAu_2Ge_2$ ($ThCr_2Si_2$ type) phase occurs only for $x \leq 2.0$. The refined lattice parameters (a = 4.4407(9) Å, c = 10.266(2) Å) showed no change (within 3σ) between x = 2.0 and x = 1.33, indicating a line compound. Single crystal diffraction on a stoichiometric reaction product converged at R1 = 1.59%, wR2 = 3.65%, GOF = 1.206. The Ca and Au atoms were refined on the Wyckoff 2*a* and 4d special positions, respectively, and Ge, on 4*e* with z = 0.3817(1). These basically agree with, but improve on, the literature data [a = 4.43(2), c = 10.23(2), z_{Ge} = 0.379], which were obtained without absorption corrections.[35]

in which Au occupies the apical site. In this case, the contradictory distribution of Au versus Ge suggests that it is the stronger Ge−Ge bonds that dominate. Figure 4 shows the densities-of-states (DOS) and the crystal orbital Hamilton population (COHP) data for $Ca_2Au_2Ge_2$. Compared with the electronic structures of other s-p bonded $ThCr_2Si_2$-type compounds,[5,34] a remarkable feature of the present parent phase is that COHP curves for network bonding exhibit only weakly bonding/antibonding characteristics over a wide energy range, − 2.0 to 2.0 eV around the Fermi energy (E_F), corresponding to a *vec* range of 8−14 (or 28−34 *vec* including Au d^{10}). Since s-p bonded $ThCr_2Si_2$-type phases are stable over a *vec* range of only 12−14,[5] the lower bonding range for the present $CaAu_2Ge_2$ phase must relate to an important participation of Au d^{10} orbitals in bonding in addition to the dominant Au−Ge interactions. This is evident in the DOS, in which the distributions of Au 5d states actually span the whole energy range [i.e., 2.5% of integrated DOS below −8.0 eV, 88.5% between −7.2 and E_F, and 9.0% above E_F].

Under rigid band assumptions, the weakly bonding or antibonding population around E_F could suggest that a structure with better optimized bonding around E_F might be found. For example, the occurrence of La_2NiAl_7 can be considered as one type of optimization of the antibonding states in hypothetical "$LaAl_4$".[34] (Another type of optimization is to create vacancies and to rearrange the network, for example, "$LaAl_{3.67}\square_{0.33}$" → La_3Al_{11}.) What Figure 4 suggests is that some 1:4 compositions around $CaAu_2Ge_2$ may be similarly optimized through the accommodation of electron-poorer elements and/or creation of vacancies under the rigid band assumptions, for instance, "$CaAu_{2.67}Ge_{1.33}$" (*vec* = 10), "$CaAu_{2.33}Ge_{1.33}\square_{0.33}$" (9.67), and "$CaAu_{2.67}Ge\square_{0.33}$" (8.67). The last two hypothetical compositions are actually close to or same as the refined compositions of crystals **1** and **4** ("$CaAu_{2.33}Ge_{1.33}\square_{0.33}$" = $Ca_3Au_7Ge_4$ ~ $Ca_3Au_{7.16}Ge_{3.84}$, "$CaAu_{2.67}Ge\square_{0.33}$" = $Ca_3Au_8Ge_3$ ~ $Ca_3Au_{8.01}Ge_{2.99}$) with reduced symmetries. So the formation of the new $Ca_3(Au,Ge)_{11}$ products can be considered to result from bonding and structural optimizations via the creation of vacancies and a rearrangement of the electronegative network of the $CaAu_2Ge_2$ phase. Although many other factors may be involved in the stability of a specific structure, for example, electronic or size factors, electronegativities, and so forth, bonding optimization appears to be dominant for the phases studied here.

Figure 5 shows the electronic structure calculated for a defect-free "$Ca_3Au_7Ge_4$ (*Imm*2)" (*vec* = 29) model, which is **1** with the M7 site fully occupied by Ge. Generally, the "$Ca_3Au_7Ge_4$" DOS is similar to that for $CaAu_2Ge_2$, but the Fermi energy in the former model is lowered by ~0.2 eV and, simultaneously, the Au d bands are broadened and thereby shifted up ~1.0 eV because of the increase in Au participation and more bonding at lower energy. Under rigid band assumptions, crystal **1**, $Ca_3Au_{7.16}Ge_{3.84}$ (*vec* = 28.5), and **2**, $Ca_3Au_{7.43}Ge_{3.57}$ (*vec* = 27.7) would locate about 0.10 and 0.24 eV to the left of Fermi energy, as marked. Notice that the Au−Au and Au−Ge COHP data change their bonding characters within this energy range, suggesting a well optimized structure in terms of bonding.

Now let us look at the Au−Au and Au−Ge bonding in crystals **3** and **4**. LMTO calculations were performed on

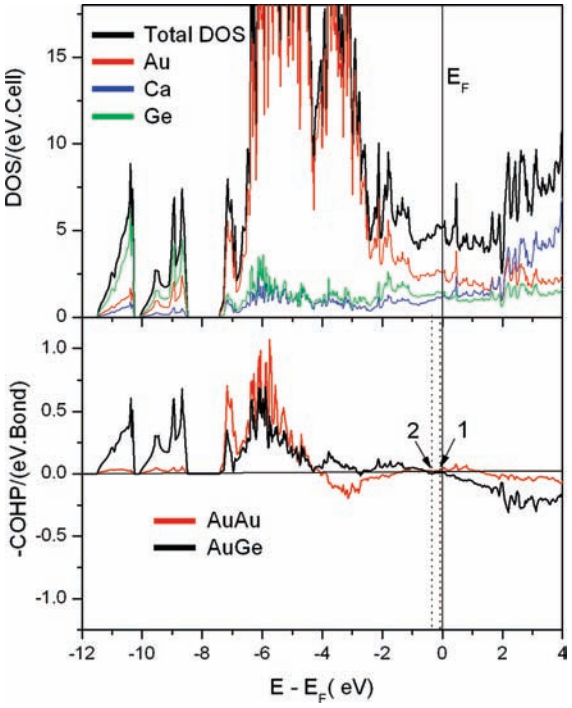

Figure 5. Densities-of-states (DOS) and crystal overlap Hamilton population (COHP) data for hypothetical $CaAu_7Ge_4$ (*Imm*2). The relative valence electron counts for crystals **1**, $Ca_3Au_{7.16(6)}Ge_{3.84(6)}$, and **2**, $Ca_3Au_{7.43(5)}Ge_{3.57(5)}$ are marked by dotted lines.

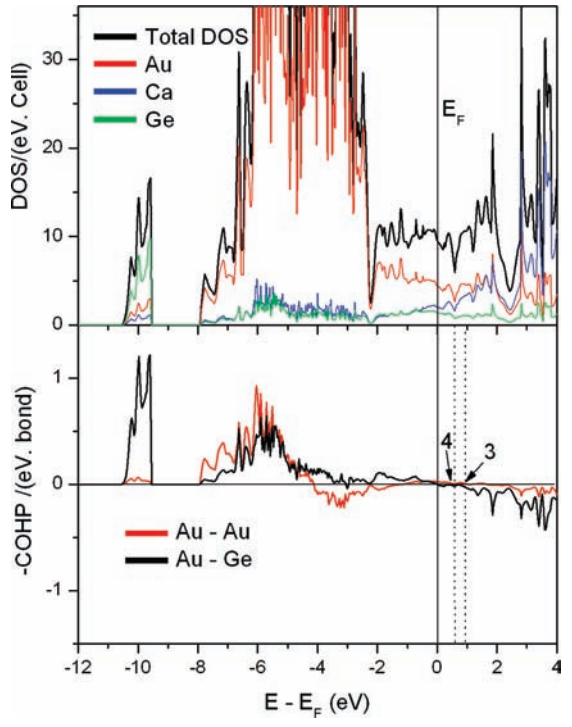

Figure 6. Densities-of-states (DOS) and crystal overlap Hamilton population (COHP) data for hypothetical $CaAu_8Ge_3$ (*Pnnm*). The relative valence electron counts for crystals **3**, $Ca_3Au_{7.50(1)}Ge_{3.50(1)}$, and **4**, $Ca_3Au_{8.01(1)}Ge_{2.99(1)}$, are marked by dotted lines.

the hypothetical structural model "$Ca_3Au_9Ge_2$ (*Pnnm*)" in which the mixed *M*6 sites in **3** and **4** were assumed to be fully occupied by Au. The DOS and COHP patterns are shown in Figure 6. Both patterns are generally similar to those shown in Figure 5, but the effect of the increasing

Au content is obvious in spite of its higher electron count, that is, E_F lies lower and the Au 5d bands are broader and closer to the Fermi energy. Under a rigid band assumption, the range of crystals **3** and **4** would fall at $\sim 0.69-0.99$ eV above E_F (as marked). Note that the bonding within this energy range is actually optimized, as expected.

Conclusions

We report here the syntheses, structures, and bonding analyses of $Ca_3Au_{\sim 7.30}Ge_{\sim 3.70}$, a centric *Imm*2 product, and $Ca_3Au_{\sim 7.75}Ge_{\sim 3.25}$, a non-centric *Pnnm* phase, both derivatives of the La_3Al_{11} structure type and new $1 \times 3 \times 1$ superstructure derivatives of $CaAu_2Ge_2$ ($ThCr_2Si_2$-type). Their structures exhibit characteristic features of both $CaAu_2Ge_2$ and Ba_2AuTl_7, which contain hexagonal and pentagonal prisms of Au/Ge polyanions, respectively. TB-LMTO-ASA band structure calculations using density functional theory reveal that the parent $CaAu_2Ge_2$ exhibits weak bonding and/or antibonding over the energy range of $\sim \pm 2.0$ eV. Under the rigid band assumptions, this allows bonding and structural optimizations for the hypothetical "$CaAu_{2.33}Ge_{1.33}\square_{0.33}$" (= $Ca_3Au_7Ge_4$) and "$CaAu_{2.67}Ge\square_{0.33}$" (= $Ca_3Au_8Ge_3$), which lie in the same energy range and are close in composition to crystals **1**−**4**, through creation and elimination of vacancies.

Acknowledgment. The authors thank K. Dennis for allowing use of the DTA Instruments. This research was supported by the Office of the Basic Energy Sciences, Materials Sciences Division, U.S. Department of Energy (DOE). The Ames Laboratory is operated for the DOE by Iowa State University under contract No. W-7405-Eng-82.

Supporting Information Available: Detailed crystallographic data for four structures in CIF form; the atomic coordinates in a non-standard setting (*Pmnn*) for crystals **3** and **4** (Table S1); the anisotropic displacement parameters for **1** and **2** (Table S2) and for **3** and **4** (Table S3), and the important interatomic distances (Table S4); the observed electron density maps of crystals **1** and **3** (Figure S1), and the DTA results (Figure S2). This material is available free of charge via the Internet at http://pubs.acs.org.